SUPPLEMENTARY MATERIAL

The 2012 Sumatra great earthquake sequence

Zacharie Duputel[1*], Hiroo Kanamori[1], Victor C. Tsai[1], Luis Rivera[2],

Lingsen Meng[1], Jean-Paul Ampuero[1] and Joann M. Stock[1].

(1) Seismological Laboratory, California Institute of Technology, 1200E. California Blvd., Pasadena, California 91125, USA.

(2) IPGS-EOST, CNRS/Université de Strasbourg, UMR 7516, 5 rue René Descartes, 67084 Strasbourg Cedex, France.

Centroid depth

The source excitation kernels of long-period fundamental mode Love waves for a strike-slip source such as the Mw=8.6 Sumatra earthquake do not vary much with depth within the first hundred kilometers (Kanamori and Given, 1981). On the other hand, the corresponding Rayleigh wave kernel values decrease with depth. This is illustrated on Fig. S15b which shows Rayleigh and Love wave seismograms at station AQU computed for two different centroid depths (10 km and 30 km). The Love waveform is very similar for different centroid depths contrarily to Rayleigh waves for which the amplitudes decrease with depth.

To obtain an estimate of the centroid depth for the Mw=8.6 mainshock, we compare directly the observed and predicted Rayleigh wave / Love wave amplitude ratios (R/L ratios) at different depths. The depths estimated at individual stations are presented on the histogram in Fig. S15a. We also

measured an average R/L ratio after amplitude equalization to Δ=90° (using the procedure of Kanamori, 1970) and azimuthal correction due to the mechanism. The comparison of the average observed and predicted R/L ratios is shown on Fig. S15a, for 3 different source models: Global CMT, W phase single-point-source solution and the double-point-source model presented in section 5 of the main text. This first order depth estimation clearly excludes the possibility of a very shallow centroid depth and suggests an optimum depth around 30 km.

Another way of estimating the centroid depth is to focus on the Rayleigh waves only and to compare the observed and predicted amplitudes at different depths for different source models. SEM synthetics were computed for a 3D earth (S362ANI and Crust2.0), for various depths between 10 km and 60 km. The optimum depth can then be defined as the one showing observed/predicted amplitude ratios closest to unity. Fig. S16 shows the amplitude ratios computed for the Global CMT and for the two-point-source model presented in section 5. Although the effect of source directivity makes this plot difficult to interpret, it seems that the optimum source depth ranges between 20 km and 40 km. This is clearly confirmed by the direct comparison between observed and predicted amplitudes shown on Fig. 7 of the main text that indicates an optimum centroid depth around 30 km.

References

Kanamori, H., 1970. Synthesis of long-period surface waves and its application to earthquake source studies—Kurile Islands earthquake of October 13, 1963. J. Geophys. Res. 75, 5011–5027.

Kanamori, H., Given, J.W., 1981. Use of long-period surface waves for rapid determination of earthquake-source parameters. Phys. Earth Planet. Inter. 27, 8–31.

Supplementary Figures

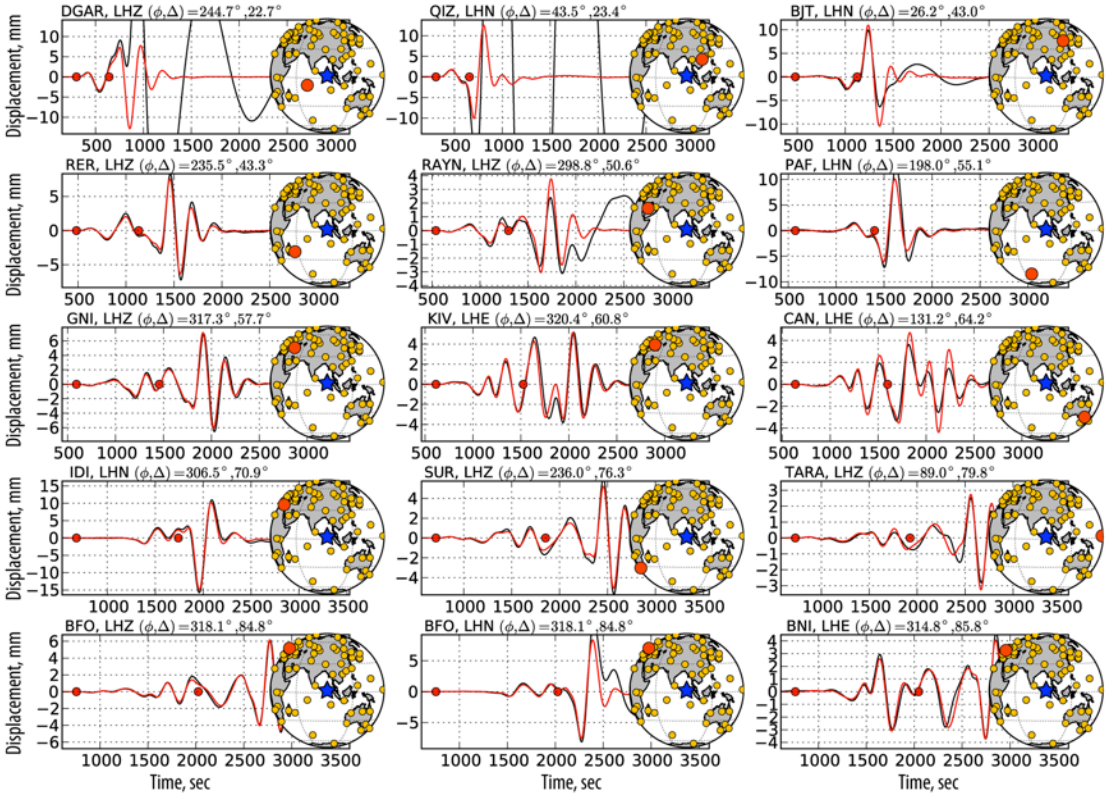

Figure S1: W phase waveform comparison for the Mw=8.6 2012 Sumatra earthquake. Examples of observed waveforms (black lines) and the corresponding synthetics (red lines) computed from the point-source W phase solution are presented. The station azimuth (ϕ) and epicentral distance (Δ) are indicated, as well as the W phase time window, bounded by red dots. W phase and later arrivals are generally well predicted at very long period. For some channels like DGAR-LHZ, QIZ-LHN, BJT-LHN or RAYN-LHZ, the surface waves are affected by instrument problems (i.e., clipping), though the W phase signal is not affected.

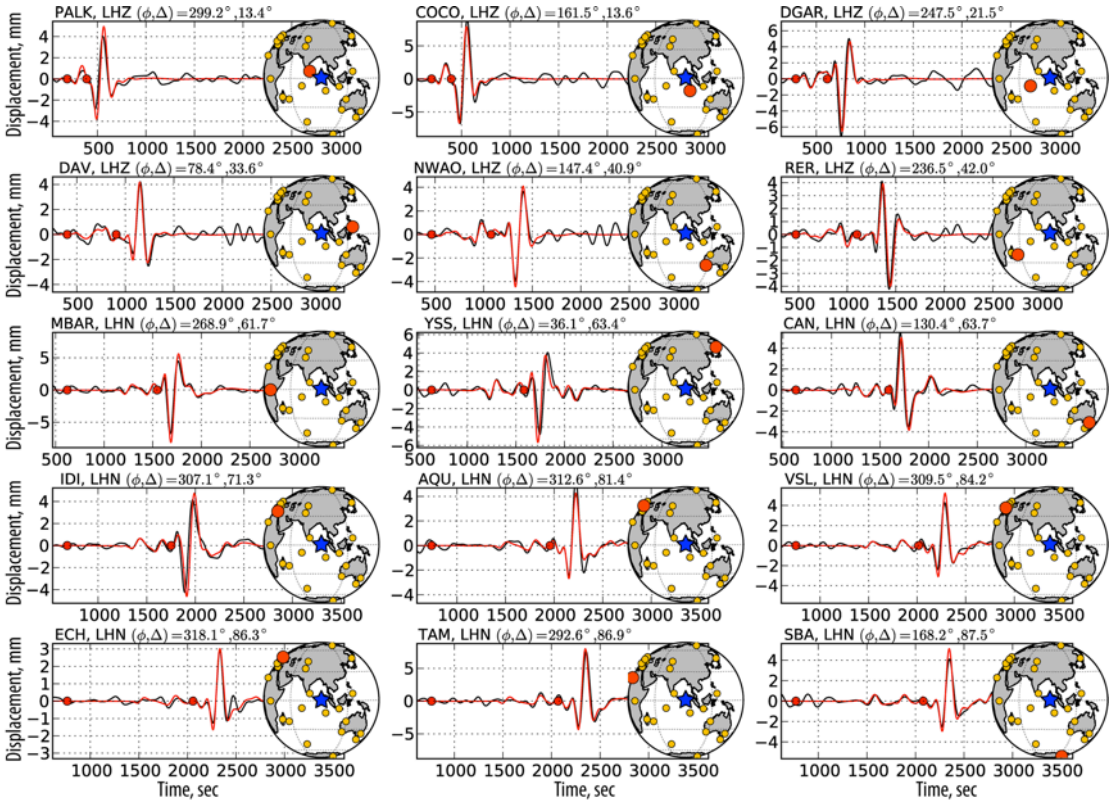

Figure S2: W phase waveform comparison for the Mw=8.2 2012 Sumatra aftershock. Examples of residual traces obtained by subtracting double-point-source SEM synthetic seismograms for the Mw=8.6 mainshock from the data (black lines) and the corresponding synthetic seismograms for the Mw=8.2 aftershock (red lines) are shown. The station azimuth (ϕ) and epicentral distance (Δ) are indicated, as well as the W phase time window, bounded by red dots. Large amplitude surface waves emerging after the W phase (i.e., fundamental Rayleigh and Love waves) are generally very well predicted by the W phase solution, even though they are not included in the inversion.

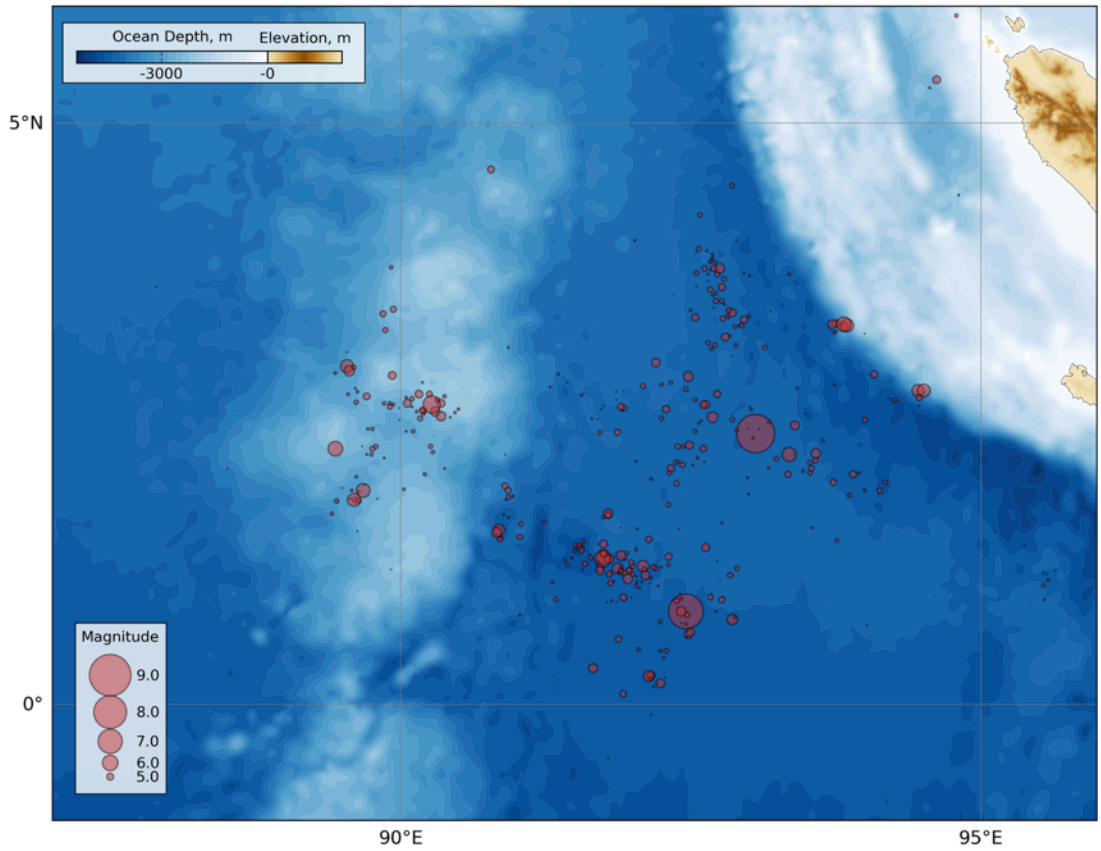

Figure S3: Distribution of the mainshock and aftershocks during the 2012 Sumatra earthquake sequence. The earthquakes hypocenter location from the NEIC catalog between 11 April 2012 and 3 May 2012 are depicted as circles. The circles radius scales linearly with the earthquake magnitude.

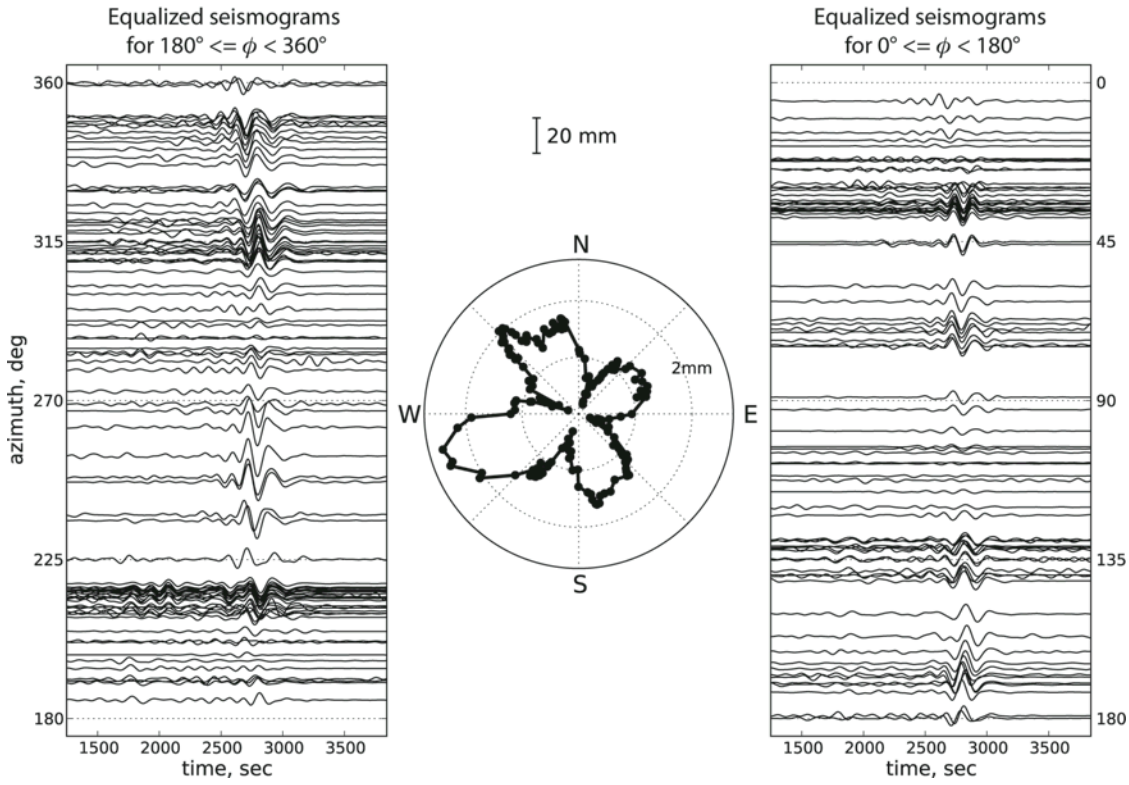

Figure S4: Equalized Rayleigh waves (R1 and R2) for the Mw=8.6 2012 Sumatra earthquake. All the seismograms are equalized to a distance of Δ_0=90°. The vertical scale gives the trace amplitude in the 100-400 s passband. The equalized seismograms are ordered as a function of the station azimuth at the source (ϕ).

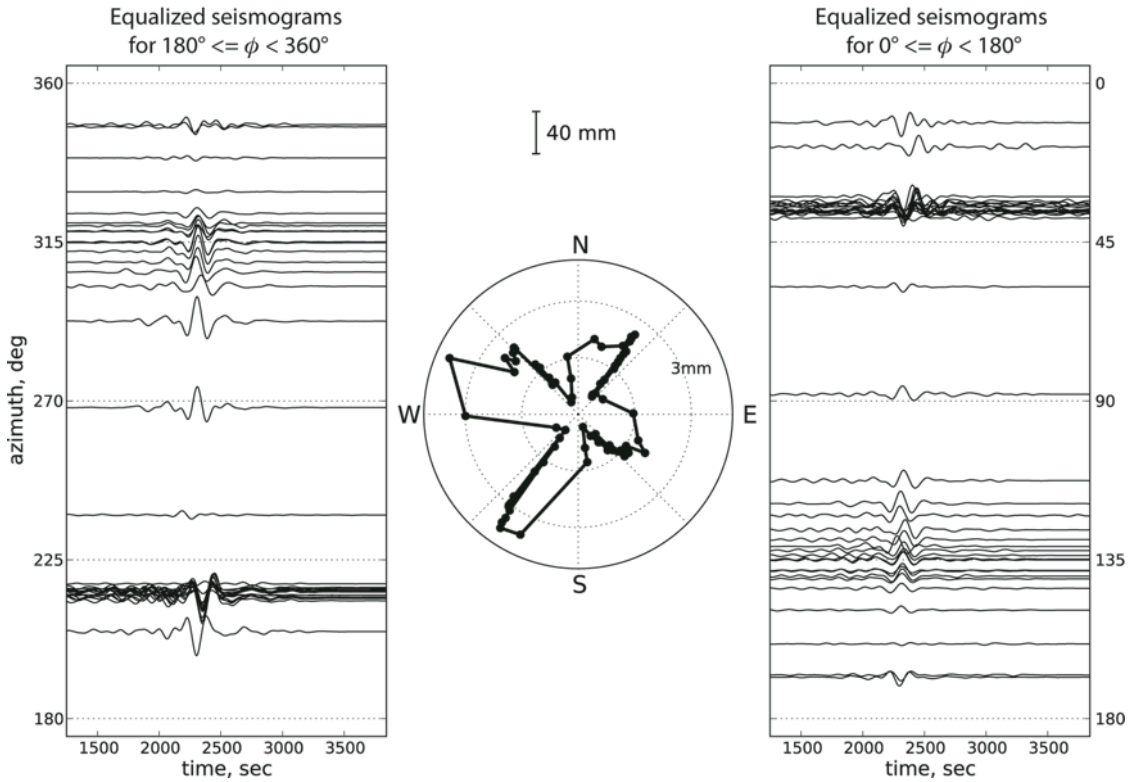

Figure S5: Equalized Love waves (L1 and L2) for the Mw=8.6 2012 Sumatra earthquake. All the seismograms are equalized to a distance of Δ_0=90°. The vertical scale gives the trace amplitude in the 100-400 s passband. The equalized seismograms are ordered as a function of the station azimuth at the source (ϕ).

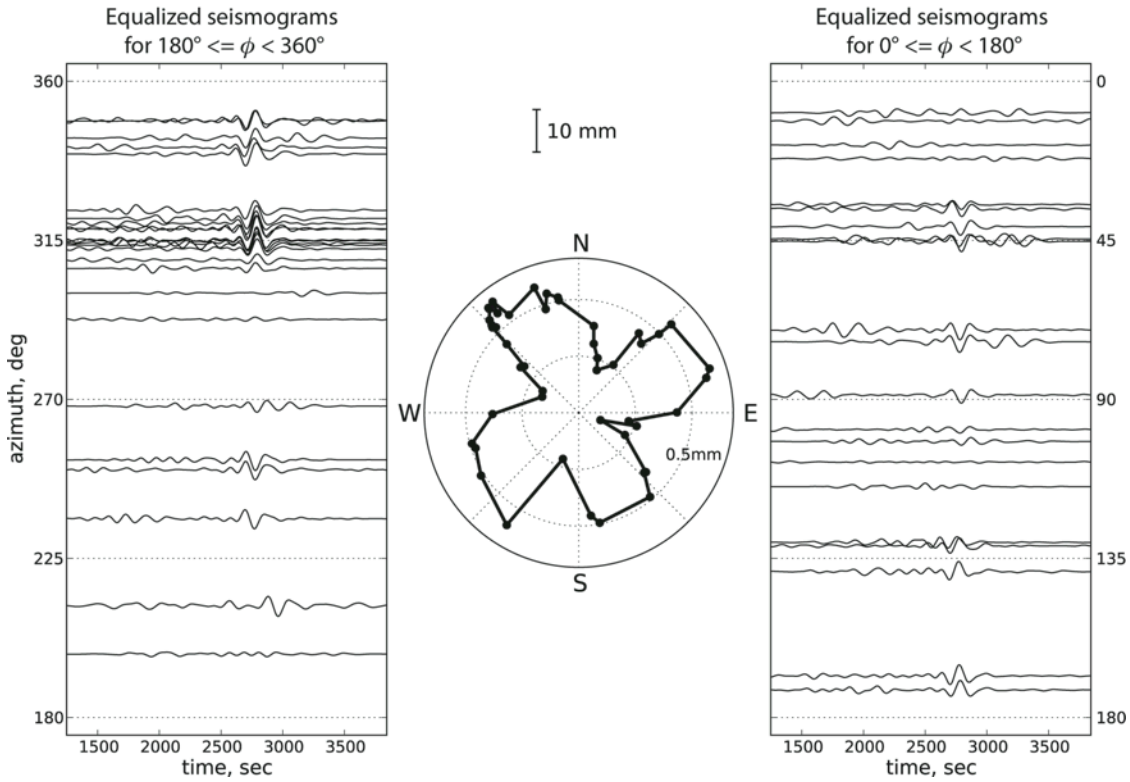

Figure S6: Equalized Rayleigh waves (R1 and R2) for the Mw=8.2 2012 Sumatra earthquake. All the seismograms are equalized to a distance of Δ_0=90°. The vertical scale gives the trace amplitude in the 100-400 s passband. The equalized seismograms are ordered as a function of the station azimuth at the source (ϕ).

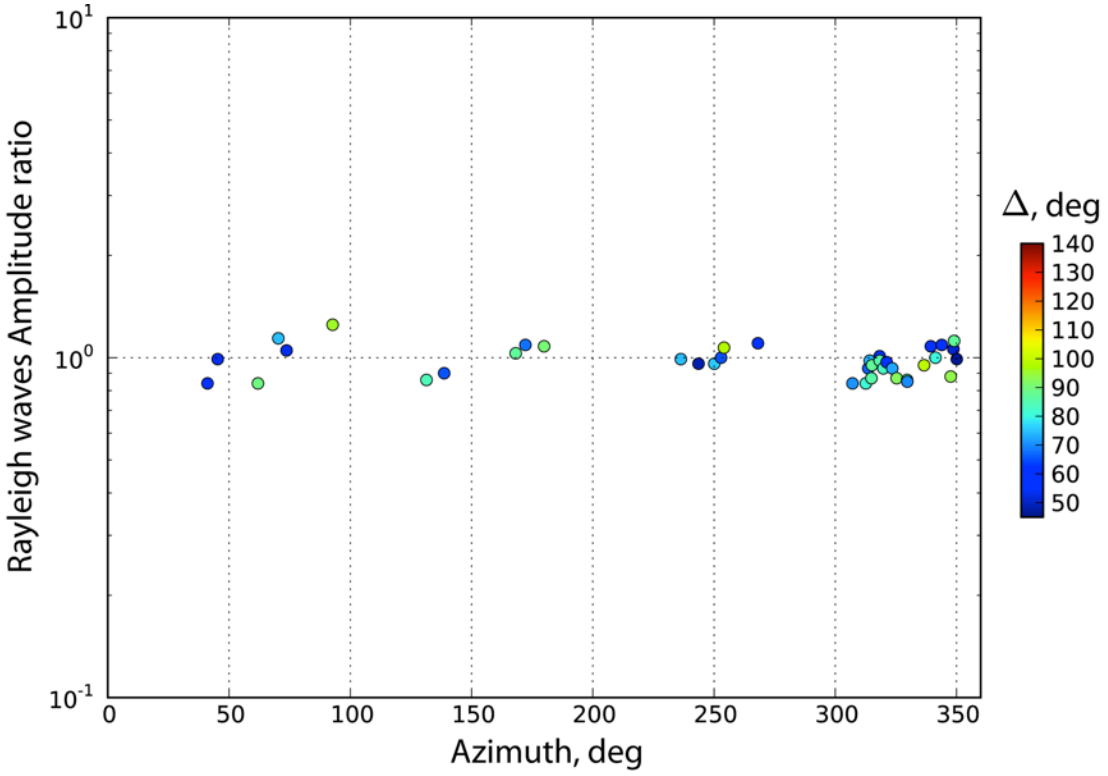

Figure S7: Long-period surface-wave directivity for the Mw=8.2 11 April 2012 Sumatra earthquake. Ratios between observed and predicted rms amplitudes measured in the 100-400 s passband are presented as circles. The circles are colored as a function of epicentral distance (Δ).

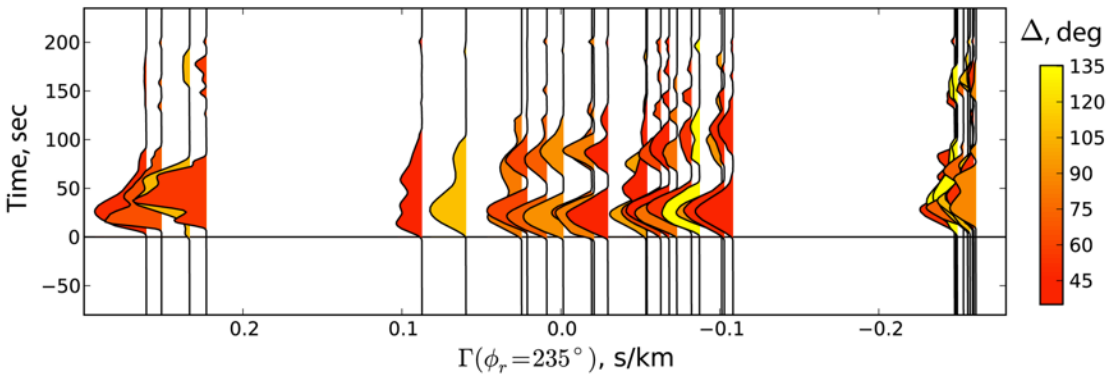

Figure S8: Rayleigh wave MRFs for the Mw=8.6 11 April 2012 Sumatra earthquake ordered assuming a rupture direction ϕ_r = 235°. The R1 MRFs obtained using the projected landweber method are ordered as a function of the directivity parameter Γ=cos(ϕ - ϕ_r)/c, where ϕ is the azimuth of the station from the epicenter, ϕ_r is the rupture direction and c is the phase velocity (here we assume ϕ_r = 235° and c = 3.8 km/s).

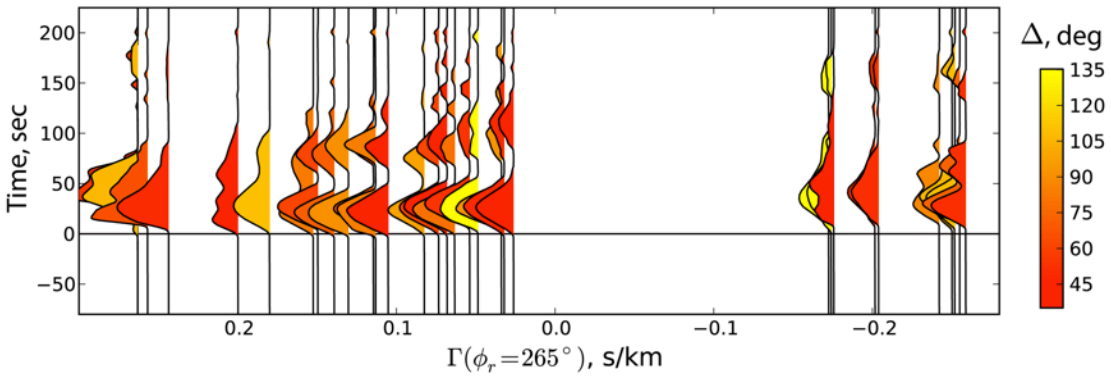

Figure S9: Rayleigh wave MRFs for the Mw=8.6 11 April 2012 Sumatra earthquake ordered assuming a rupture direction ϕ_r = 265°. The R1 MRFs obtained using the projected landweber method are ordered as a function of the directivity parameter Γ=cos(ϕ - ϕ_r)/c, where ϕ is the azimuth of the station from the epicenter, ϕ_r is the rupture direction and c is the phase velocity (here we assume ϕ_r = 265° and c = 3.8 km/s).

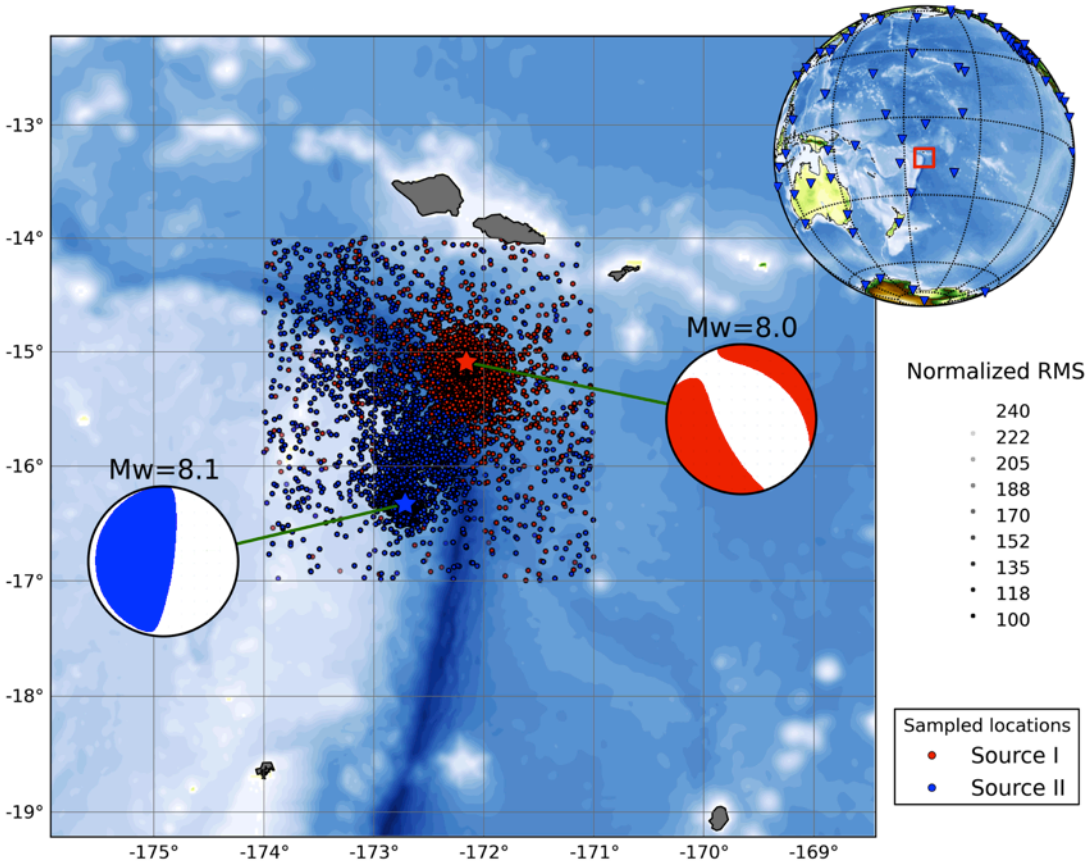

Figure S10: Example of multiple-point-source inversion result for the Mw=8.1 2009 Samoa earthquake. Explored latitude and longitude are shown in red for source I (first subevent) and in blue for source II (second subevent). Transparency indicates the rms misfit normalized by its minimum (in percent). Higher sampling is performed in regions associated with smaller rms misfits. The red and blue stars indicate respectively the optimum locations for source I and II.

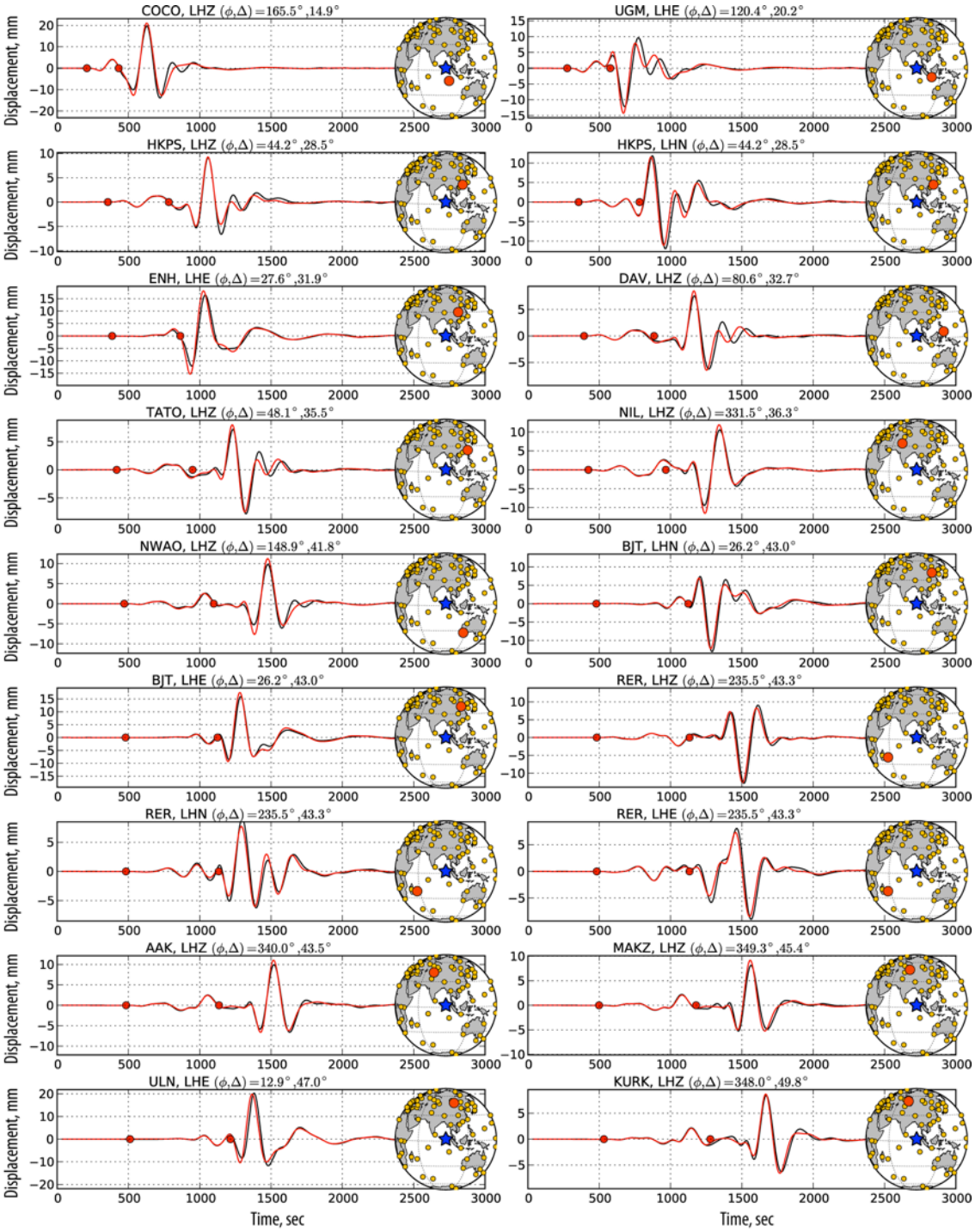

Figure S11: Waveform fits for the double-point-source model. Examples of observed waveforms (black lines) and the corresponding synthetics (red lines) computed from the two-point-source model solution are presented. The station azimuth (ϕ) and epicentral distance (Δ) are indicated, as well as the W phase time window, bounded by red dots.

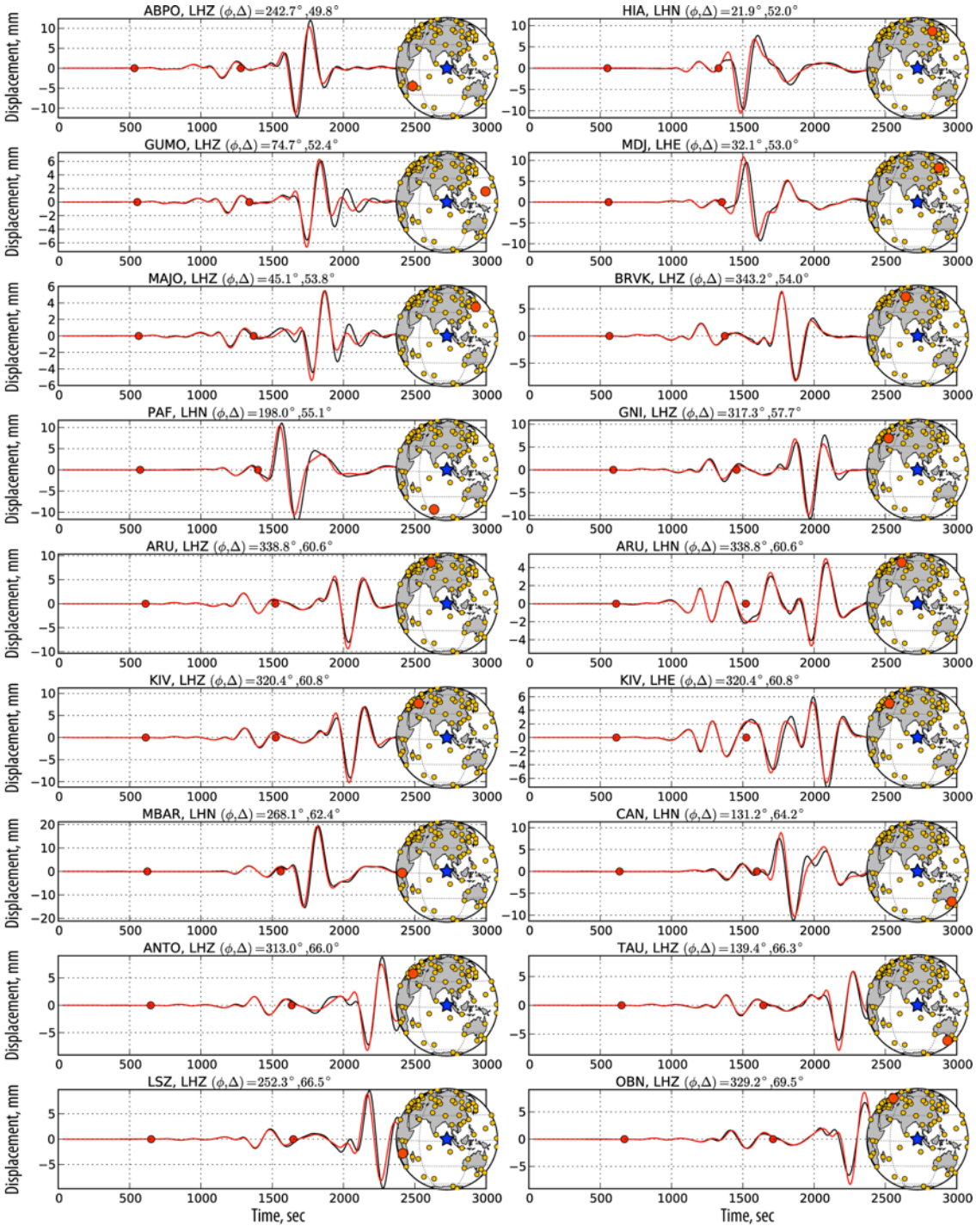

Figure S12: As in Fig S11.

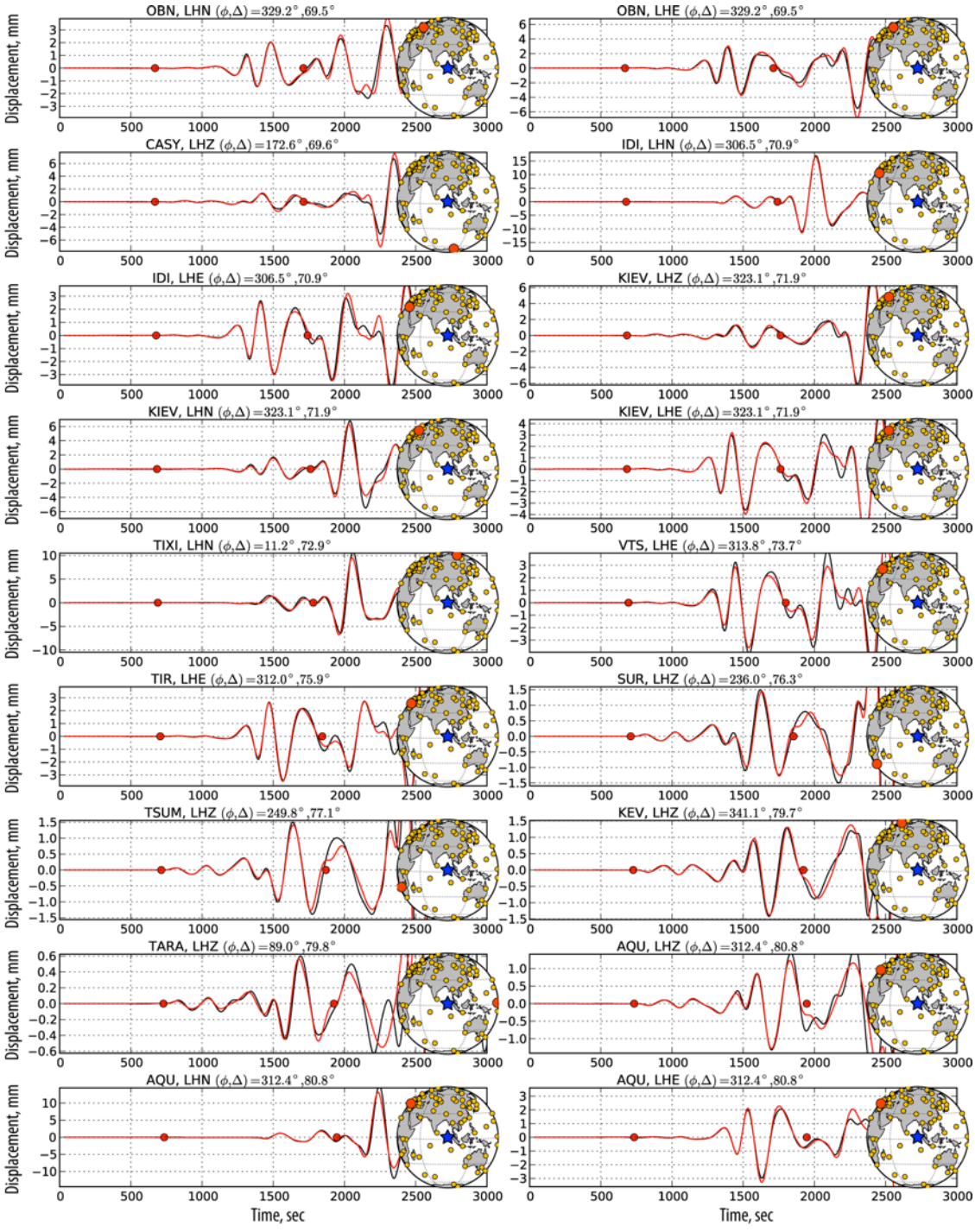

Figure S13: As in Fig S11.

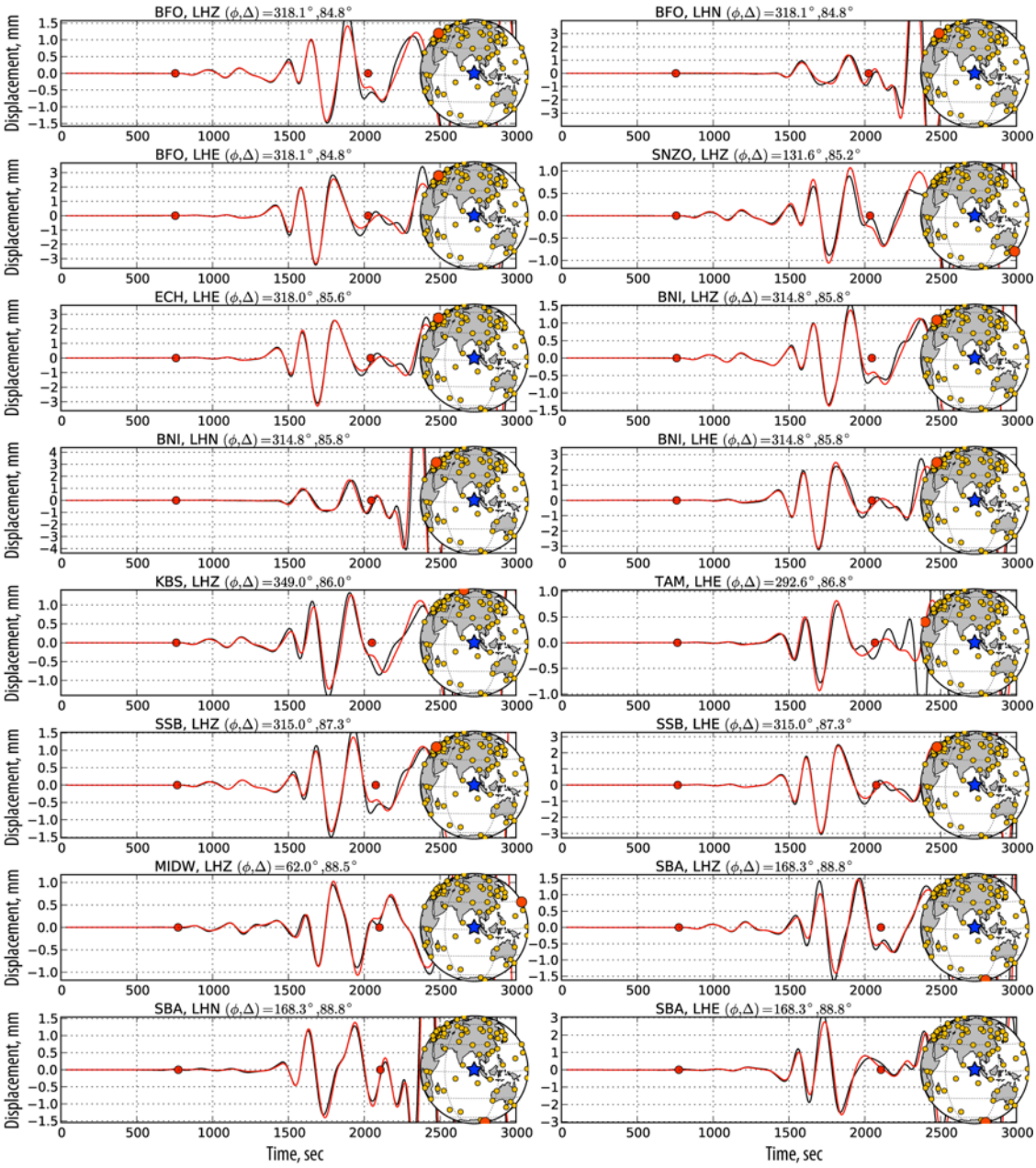

Figure S14: As in Fig S11.

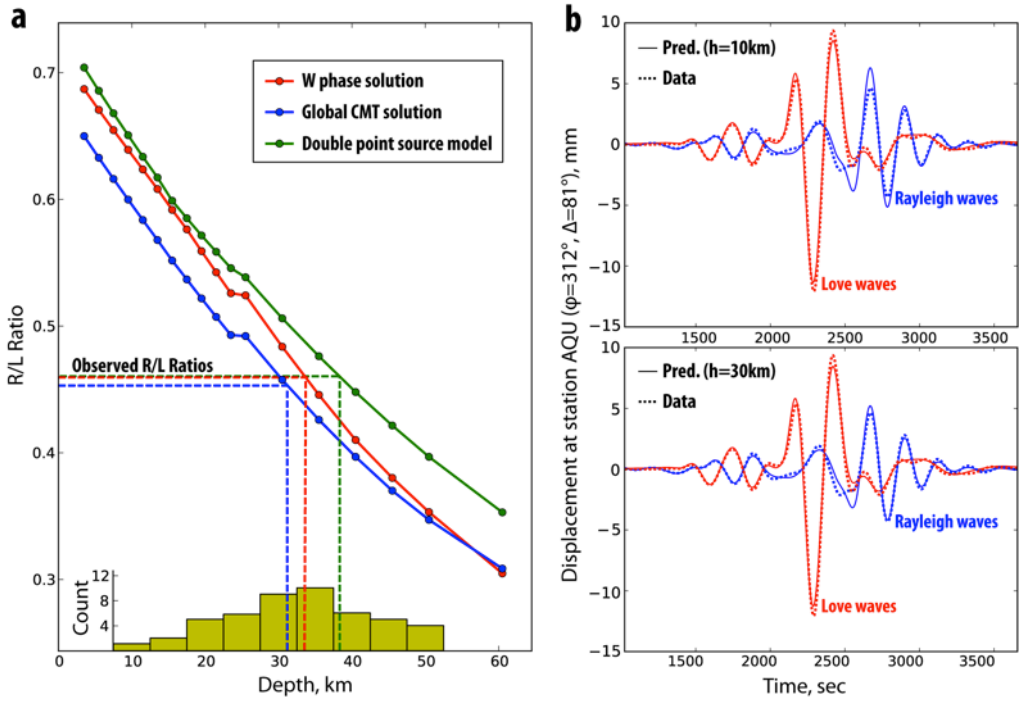

Figure S15: Variation of Rayleigh-wave and Love-wave amplitudes as a function of depth. **a.** Rayleigh/Love wave amplitude ratios. The observed average amplitude ratios (dashed lines) are compared with the predicted average amplitude ratios computed at different depths for different source models (continuous lines). The depths estimated at individual stations are summarized on the histogram at the bottom. **b.** Observed and predicted waveforms for the two-point-source model at centroid depths of 10km and 30km.

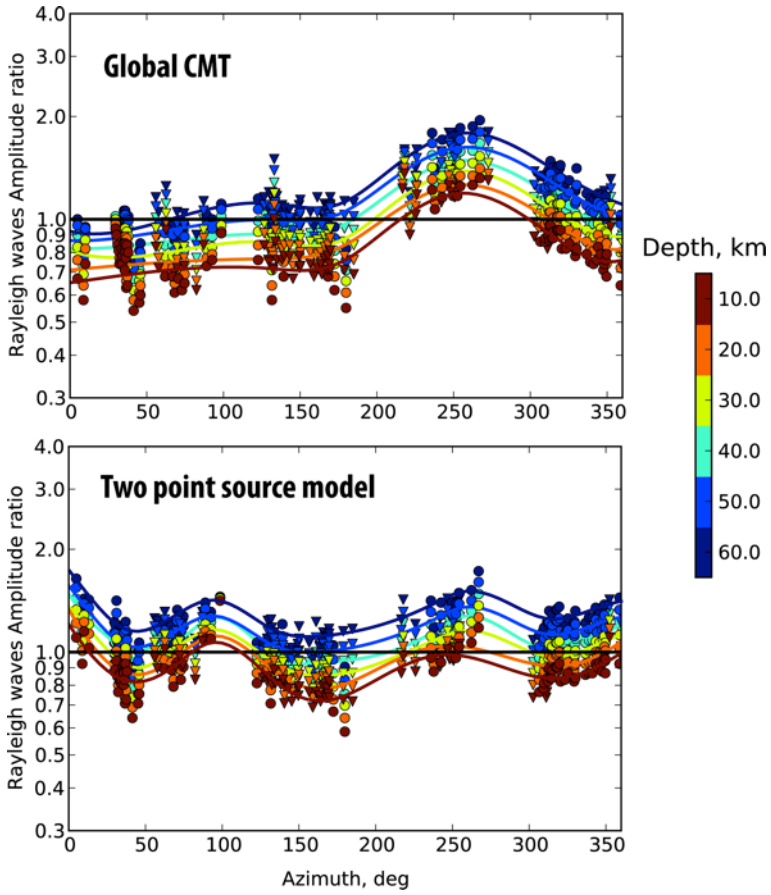

Figure S16: Long-period Rayleigh-wave amplitude variation with depth. Observed / predicted amplitude ratios have been measured in the 200s-600s passband assuming the Global CMT and the two-point-source models. R1 and R2 Rayleigh wave trains are presented respectively using circles and triangles. The amplitude ratios have been computed assuming different centroid depths indicated by the colors. Colored lines are smoothed amplitude ratio measurements for each depth.

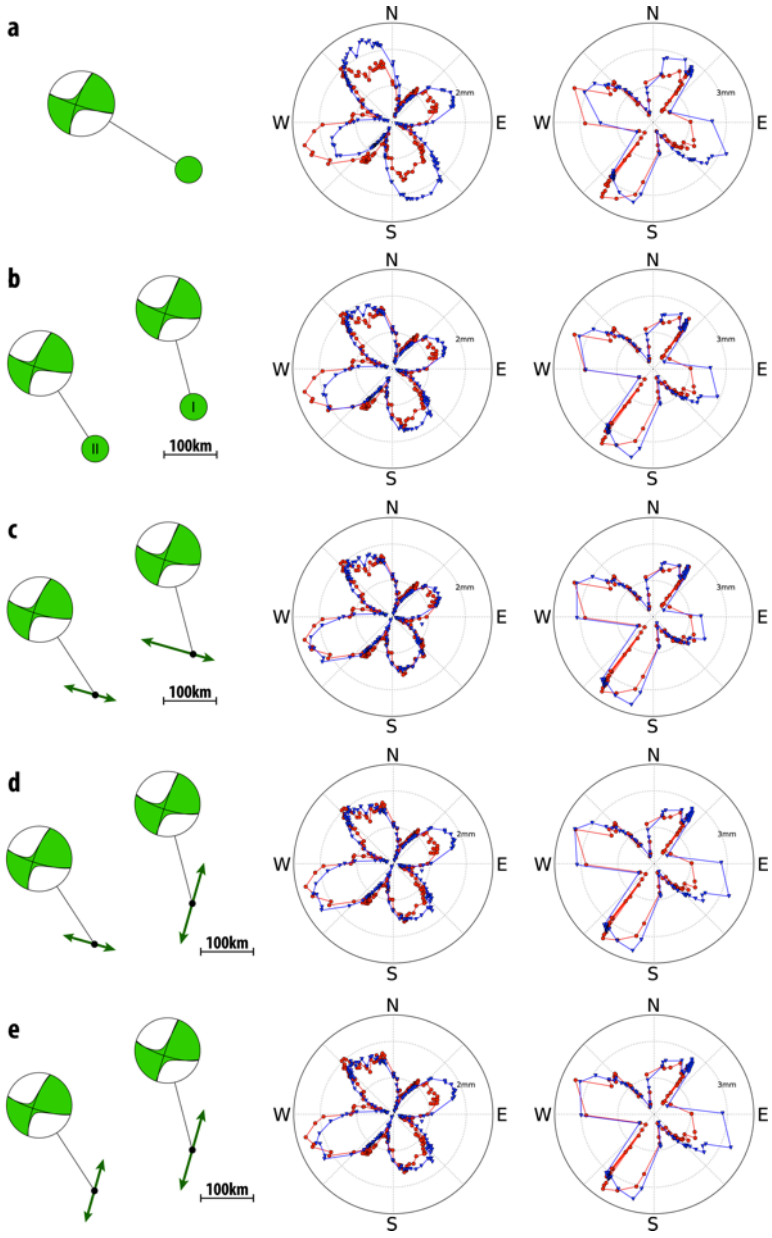

Figure S17: Examples of observed and predicted surface-waves radiation patterns for simple rupture models (uniform slip, horizontal rupture propagation). Comparison of observed (red circles) and predicted (blue triangles) equalized amplitudes for R1, R2 (middle) and G1, G2 (right). **a**. Single-point-source model. **b**. Two-point-source model. **c**. Optimum model with two parallel WNW-ESE bilateral ruptures. **d**. Example of two orthogonal NNE-SSW and WNW-ESE bilateral ruptures. **e**. Example of two parallel NNE-SSW bilateral ruptures.

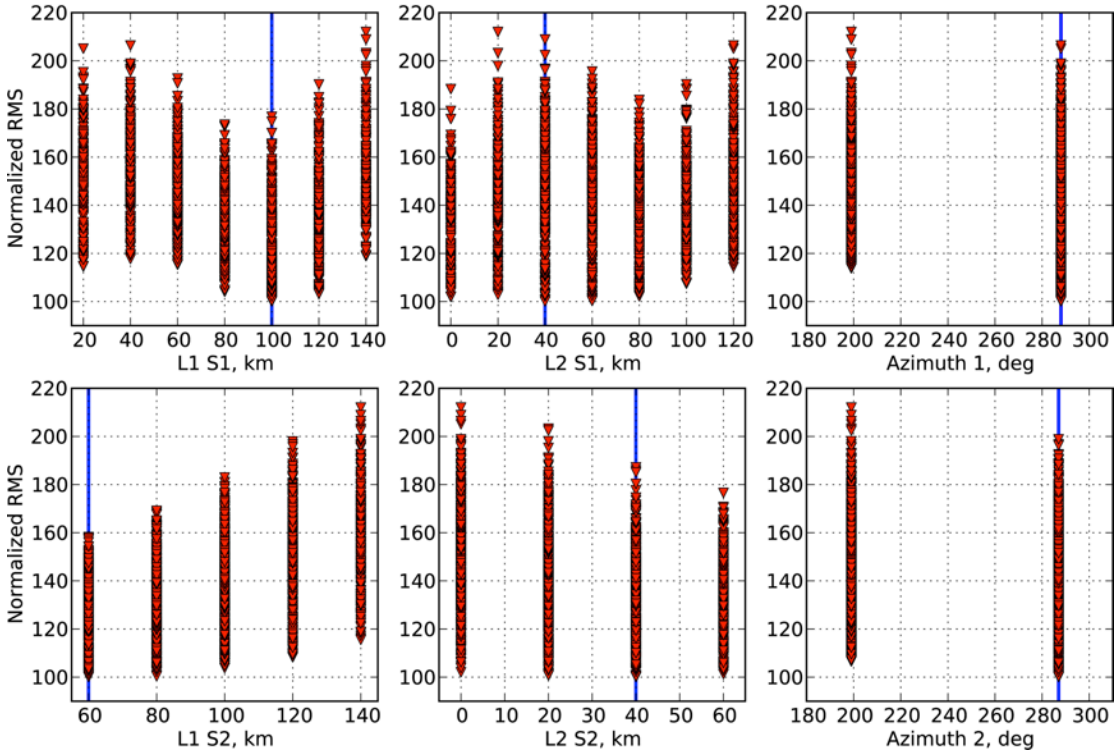

Figure S18: Summary of explored finiteness parameters for the Mw=8.6 2012 Sumatra earthquake. Rupture lengths (L1 and L2) and azimuths are regularly sampled for source I (first subevent, top 3 panels) and for source II (second subevent, lower 3 panels). Blue lines indicate the optimum set of parameters.